J Mater Sci (2019) 54:6088–6097

Ceramics

Microwave-power-enabled tuning of NiCo double hydroxide nanostructures

Bin Luo[1], Xiong Zhang[2], Tian Xie[3], Yanping Zhou[1,*], and Kama Huang[1]

[1] College of Electronics and Information Engineering, Sichuan University, Chengdu 610065, Sichuan, China
[2] School of Chemical Engineering, Sichuan University, Chengdu 610065, Sichuan, China
[3] State Key Laboratory of Efficient Utilization for Low Grade Phosphate Rock and Its Associated Resources, Wengfu Group, Guiyang 550014, China

Received: 15 October 2018
Accepted: 3 January 2019
Published online: 14 January 2019

ABSTRACT

Microwave heating has been widely used to enhance the fabricating rate of nanomaterials in the past few decades. However, the application of interaction between microwave and chemical reaction in tuning nanomaterials morphology is yet to be explored, while strategies to manipulate material nanostructures are of great importance for enhanced function. In this work, we demonstrate the potential of microwave in tuning the morphology of nanostructured NiCo DHs by accurate temperature control through the precise design of microwave reacting system. We find that 200-W microwave irradiation gives yield to unique flower-on-sheet hierarchical structure of NiCo DHs, while microspheres are derived from oil-bath heating. Microwave power is found to play a vital role in the tuning process. When microwave power decreases to 50 W, assembled nanoflakes are obtained; when microwave power increases to 300 W, microspheres are obtained. Further, fluid permittivity is monitored and field intensity in the reacting region is simulated and found to increase with time. Taken together, it is proposed that field-induced de-solvation possibly exists and is the main tuning mechanism. When tested as electrode materials in supercapacitor, products obtained from 200 W microwave treatment show enhanced storage capacities, especially at high current density.

Introduction

Controllable fabrication of hierarchical nanostructures has received intensive research interest during the past decades due to its crucial impact on performance of functional nanomaterials in various areas such as energy storage [1, 2], catalysis [3, 4], sensor [5, 6]. Up to now, much effort has been devoted to synthesize various hierarchical nanostructures with enhanced performance, such as nanochains [7, 8], nanosheets [9, 10], hollow

Address correspondence to E-mail: zhouyanping87@126.com

https://doi.org/10.1007/s10853-019-03324-y

microspheres [11, 12], inter-connected 3D network [13, 14]. Generally, templates [15, 16] and surfactants [17, 18] are effective strategies to direct the formation of different nanostructures, which usually involve either tedious template removing process or environmental-unfriendly chemical reagents. More importantly, there are some cases in which surfactants are not desirable due to the consequent carbon derived from their decomposition. Therefore, tuning the morphology of nanomaterials in a simple and green way without the use of any template or surfactant is highly desired, but yet remains challenging.

Microwaves (MW) are electromagnetic waves with frequencies ranging from 0.3 to 300 GHz, which can heat materials via dielectric loss other than heat convection as in the conventional heating process. This unique heating mechanism brings great advantages in nanomaterials preparation such as reducing the synthesis time (e.g., from hours or even days to minutes), facilitating formation of nanoparticles with smaller size and more homogeneous size distribution, enhancing the yield [19–24]. As such, with the demand for green chemistry in both academia and industry, microwave heating is emerging as a promising heat source and has been widely applied in synthesis of functional nanomaterials [25, 26]. In particular, microwave heating has shown special benefit for fabrication of electrode nanomaterials with enhanced performance [27–30]. For example, Yan et al. [31] reported microwave-assisted preparation of $LiCoO_2$ in 5 min, which gave yield to $LiCoO_2$ nanoparticles with one-tenth diameter of those prepared by conventional heating method, thus exhibiting superior lithium storage capability. Liu et al. [32] demonstrated that microwave heating can hinder the formation of $LiMnO_2$ or $LiMn_2O_3$, thus favorable for getting $LiMn_2O_4$ with higher purity for high-performance lithium storage. However, most of these systems focused on effect of microwave on particle size or phase purity, etc.; effect of microwave on hierarchical nanostructure of electrode materials is yet to be demonstrated.

In this work, through the precise design of microwave reaction system, we report microwave-power-enabled tuning of nickel cobalt double hydroxides (NiCo DHs) hierarchical nanostructures. As typical 2D materials, NiCo DHs have attracted much attention for application as high-performance electrode materials in supercapacitors or as precursors for preparation of 2D nickel cobalt oxides for lithium/sodium ion batteries [33–35]. We demonstrated that unique NiCo DHs nanoflower-on-sheet hierarchical structures were obtained when 200-W microwave irradiation was applied, while microspheres composed of nanosheets were derived from oil bath with the same temperature program. When the microwave power was adjusted to 50 W and 300 W, the nanostructure was tuned to assembled nanoflakes and microspheres, respectively. De-solvent effect that resulted from microwave-field-induced vigorous vibration of polar molecules was proposed to play key roles in the controllable synthesis. When tested as electrode materials in supercapacitor, the flower-on-sheet nanostructure showed enhanced energy storage capacities.

Experimental

Materials

All the chemicals were purchased from Aladdin Chemical Corporation, and of analytical grade.

Method

Synthesis of NiCo DH hierarchical nanostructure

In a typical procedure, 4.8 mmol of $Co(NO_3)_2$ and 2.4 mmol $Ni(NO_3)_2$ were dissolved in 72 mL DI water, to which 48 mL EG was added. The mixture was stirred vigorously for 30 min, and placed in a self-designed microwave chemical reaction system. The microwave heating chamber was equipped with a microwave solid-state oscillator as the microwave power source and a fiber optic thermometer to measure the system temperature. Urea was added when the solution temperature reached 100 °C. Afterward, the mixture was exposed to microwave irradiation for 30 min at a power output of 50 W, 200 W, 300 W, respectively. The system temperature was regulated within 100 ± 0.3 °C by circulating cooling oil that is transparent to microwave. Following the heat treatment, the precipitation was harvested, washed by DI water and ethanol for several times. The final products were dried in a vacuum at 60 °C for 24 h to obtain the NiCo DH (named as NiCo DH-50 MW, NiCo DH-200 MW, NiCo DH-300 MW, respectively) powders for characterization and electrochemical measurement. For comparison, oil-bath experiment

was done with the same recipe and under the same heating program with 200-W microwave irradiation. The product was designated as NiCo DH-OB.

Materials characterization

The morphologies of the products were examined under a field emission scanning electron microscopy (FESEM, Hitachi, S3400, Japan) and a high-resolution transmission electron microscopy (HRTEM, JEOL, JEM-2010, Japan). X-ray diffraction on a diffractometer (XRD, Haoyuan, DX-2700, China) using Cu Kα radiation at 40 kV and 30 mA was used to characterize the crystalline structure of NiCo DH samples. The Brunauer–Emmett–Teller (BET) surface area was determined from N_2 adsorption/desorption isotherm at 77 K using an automated surface area & pore size analyzer (Quantachrome NOVA 1000e apparatus).

Permittivity measurement and field simulation

The permittivity of the reaction fluid under different reaction times was measured by the transmission reflection method. Firstly, S_{11} and S_{21} values were obtained from power meters. Afterward, permittivity was deduced from S_{11} and S_{21} values based on neural network, which were further applied to calculate electromagnetic field distribution in the fluid during multi-physical fields simulation.

Electrochemical measurements

The electrochemical tests were conducted on a CHI 660E electrochemical workstation (Shanghai Chenhua Instrument Co, China) under a three-electrode configuration with a saturated Hg/HgO electrode as the reference electrode, and a graphite rod as the counter electrode in 6 M KOH aqueous solution. The working electrode was fabricated by mixing NiCo DH, acetylene black and poly (vinyldifluoride) in *N*-methylpyrrolidinone at a weight ratio of 8:1:1. The mixture was loaded on the Ni foam substrate (1 cm × 1 cm) and dried at 60 °C for 24 h. Then, the electrode was pressed under 10 MPa for 30 s. The mass loading of active material was around 3.8 mg. The specific capacitance (SC) was calculated from the galvanostatic charge–discharge curves as follows:

$$C = \frac{I\Delta t}{\Delta V \mathrm{m}}$$

where C, I, Δt, ΔV and m are the SC ($F\ g^{-1}$), the discharge current (A), the discharge time (s), the discharge potential range (V), and the mass of the active material (g), respectively. The electrochemical impedance spectroscopy (EIS) measurement was taken at open-circuit potential with a frequency range from 0.01 to 100 kHz, and an alternating current voltage of 5 mv amplitude.

Results and discussion

To study the specific effect of microwave on the hierarchical structure of nanomaterials, temperature difference between reactions under microwave heating and oil bath should be avoided. Therefore, a self-made microwave chemical reaction system was applied for the synthesis, whose illustrating scheme is shown in Fig. 1a. Generally, this microwave reaction system has the following advantages. Firstly, microwave solid-state oscillator was used as the microwave source instead of magnetron, enabling precise control of stable microwave power and frequency output during the whole reacting period, which is highly desirable for investigating the mechanism of microwave-enhanced synthesis. Secondly, it is known that the performance of commonly used thermometers such as thermocouple thermometer would be influenced by microwave field thus not suitable for temperature measurement under microwave field. Hence, herein a fiber optic thermometer was applied to measure the temperature with higher accuracy. Thirdly, circulating cooling oil that is transparent to microwave is introduced as a new strategy to control the system temperature other than tuning the microwave output power or working/resting time [21, 36]. As such, continuous microwave irradiation at constant power and constant reacting temperature was realized at the same time. Due to the subtle design of microwave reaction system, the temperature curves of samples exposed to microwave heating at 200 W and oil bath could be regulated to be almost the same, with data shown in Fig. 1b.

After reacting for 30 min, precipitations were harvested from both microwave reaction system and oil-bath reaction system. The yields were measured to be of no significance difference, indicating that microwave irradiation did not enhance the reacting rate.

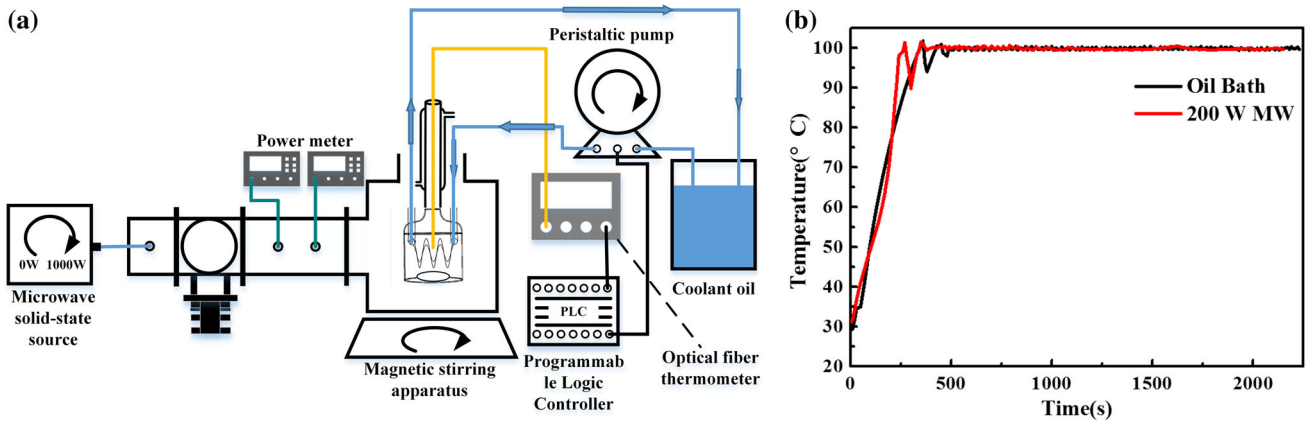

Figure 1 **a** Schematic illustration of the self-made microwave heating chamber; **b** sample temperature curves under microwave heating at 200 W and oil bath.

Figure 2 shows the XRD spectra of the as-synthesized products. Characteristic peaks located at 12.1°, 24.5°, 33.1° and 59° corresponding to the (003), (006), (101) and (110) diffraction planes of α-phase NiCo DH were observed, indicating well-crystalized α-phase NiCo DH were obtained, named as NiCo DH-200 MW and NiCo DH-OB, respectively [12, 37]. Their morphologies were examined under FESEM and TEM, with results of NiCo DH-OB shown in Fig. 3a–c and results of NiCo DH-200 MW shown in Fig. 3d–f. Obviously, the morphologies of the two samples were totally different though the temperature programs in both reacting systems were the same. Oil-bath method gave yield to NiCo DH-aggregated microspheres composed of nanosheets, which were like the morphologies of other NiCo DHs

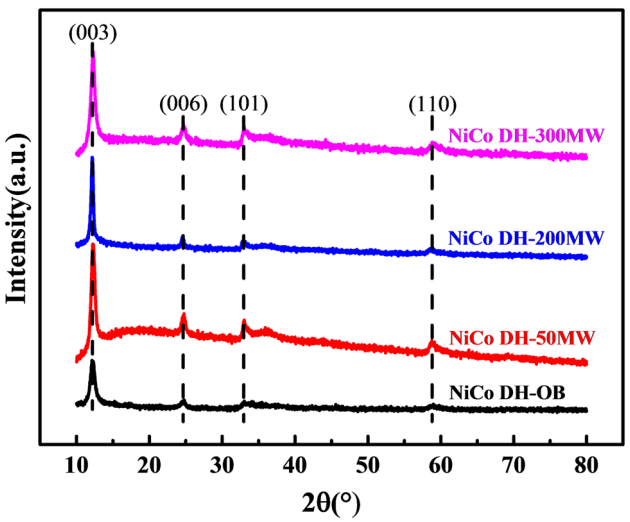

Figure 2 XRD spectra of the products obtained from different microwave power irradiations and oil baths, respectively.

derived from microwave synthetic methods reported in the literature [38, 39]. Surprisingly, NiCo DH obtained from 200-W microwave irradiation was well-dispersed nanoflowers with diameter around 200–300 nm anchored on nanosheets of around 2–3 μm width. The surface areas of the NiCo DH-OB and NiCo DH-200 MW were determined to be 32 and 57 $m^2 g^{-1}$, respectively, with pore size distributions of both being centered at 4 nm (see BET data in the supporting information, Fig. S1). The unique flower-on-sheet hierarchical nanostructure combines the advantages of 2D nanostructure and 3D nanostructure. The 2D nanosheets facilitate large surface area and continuous electron transportation path, while the 3D nanoflowers that anchored on the 2D nanosheets could effectively prevent their aggregation, which were both very desirable for electrode materials to show high storage capacity and good stability.

Subsequently, to study the mechanism for microwave-enabled tuning of NiCo DH nanostructure, products harvested after reaction for 10 min were examined under FESEM and TEM firstly. As shown in Fig. 4 well-dispersed nanosheets were obtained under 200-W microwave irradiation after 10 min, while assembled nanosheet clusters were obtained in oil-bath system under the same temperature condition, suggesting that microwave field played a vital role in dispersing the NiCo DH nuclei at the initial reaction stage. As known, under microwave field, water molecules vibrated more vigorously than EG molecules due to their higher polarity and smaller weight. Attributed to this vigorous vibration, certain water molecules would be removed from the nuclei

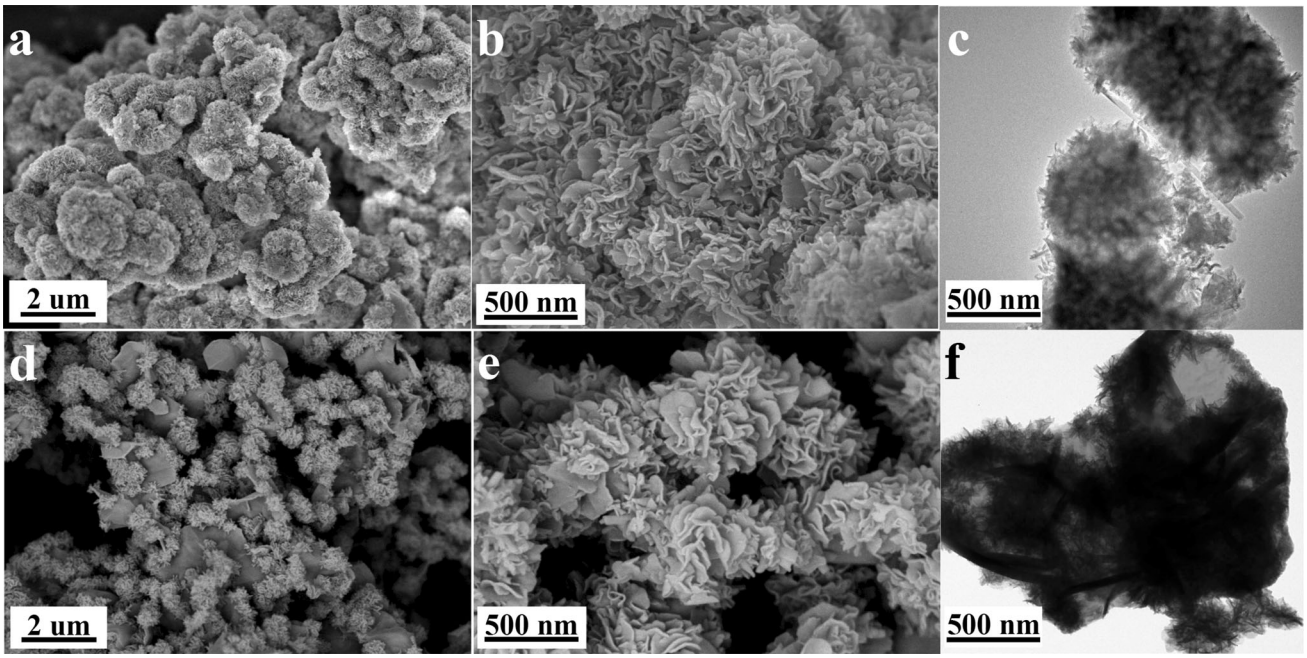

Figure 3 FESEM (**a**, **b**, **d**, **e**) and TEM (**c**, **f**) images of the as-synthesized NiCo DHs harvested from oil-bath method (**a**–**c**) and 200-W microwave irradiation (**d**–**f**), respectively.

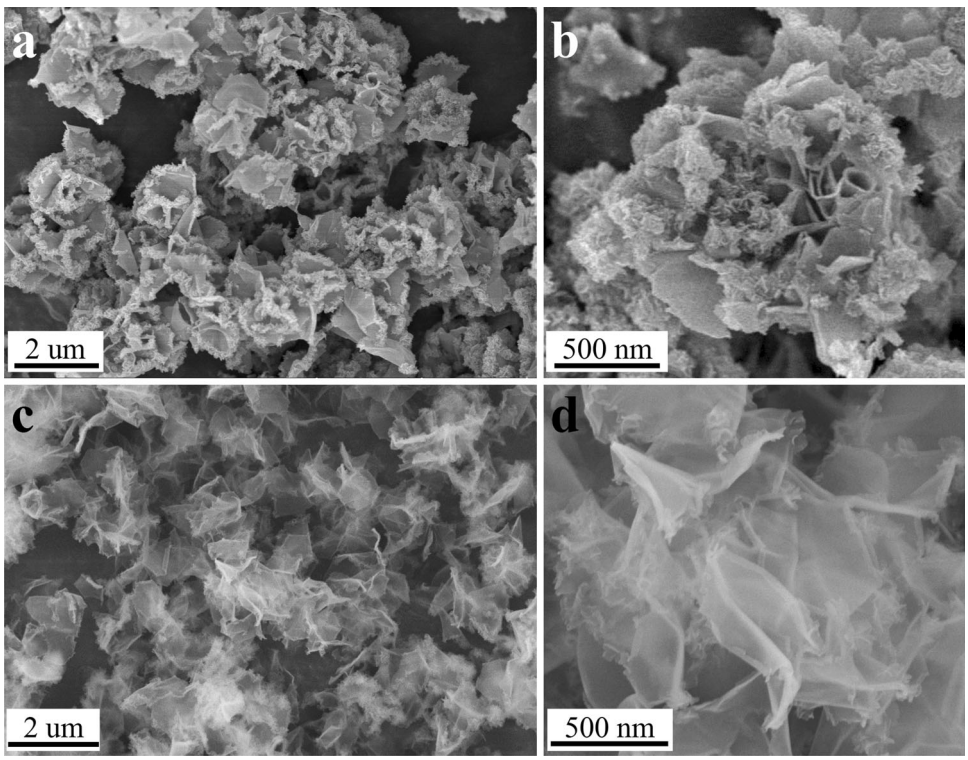

Figure 4 FESEM images of NiCo DHs harvested after reaction for 10-min oil-bath heating (**a**, **b**) or under 200 W microwave heating (**c**, **d**).

and replaced by EG molecules, causing decrease in hydrophobic force between nuclei and preventing hydrophobic aggregation. Secondly, effect of microwave power was investigated. Figure 5 shows FESEM images and TEM images of NiCo DHs harvested from 50 W microwave irradiation and 300 W microwave irradiation after reaction for 30 min, respectively. As can be seen, the flower-on-sheet

nanostructure as obtained from 200 W microwave radiation was not observed. Instead, nanoflakes for 50 W microwave treatment and assembled microspheres for 300 W microwave treatment were obtained. This indicated that microwave power was crucial for the fabrication of the unique flower-on-sheet nanostructure; low microwave intensity was responsible for the formation of 2D nanosheets, and high microwave intensity caused the formation of assembled 3D flower. It is probably that under higher microwave power (e.g., 300 W), both water and EG molecules were partly removed from nuclei, leading to nuclei aggregation. Thirdly, field intensity in fluid area during the reaction was monitored. Permittivity values of the reacting fluid at different reaction times were measured, with data shown in Table S1. As the reaction went on, tangent loss value decreased due to the larger decrease in real-part value than imaginary-part value, indicating decreasing microwave absorption, which further resulted in increased field intensity in the fluid area during reaction, as shown in Fig. 6. The average and maximum electric field intensities at different reaction times under different microwave powers are shown in Table S2 (see supporting information). At the initial stage (t = 0 min), for microwave irradiation at 50 W, 200 W and 300 W, the average electric filed intensities were 321, 642 and 786 V/m, respectively. After reaction for 20 min (t = 20 min), the values increased to 413, 826 and 1012 V/m, respectively. It is worth to note that the field intensity under 200-W microwave irradiation at t = 20 min was higher than that under 300 W at t = 0 min, leading to the initiation of flower growing on the 2D sheets.

Taken together, the mechanism for microwave-enabled nanostructure tuning is proposed as follows, with diagram shown in Fig. 7. In the absence of microwave, since the ratio of water to EG was 6:4, water overwhelmed in the solvation layer around NiCo DHs nuclei, resulting in nuclei aggregation driven by hydrophobic force. After further orientated attachment growth, NiCo DHs microspheres composed of nanosheets were obtained. However, when microwave was introduced, de-solvation would happen as both water and EG molecules are polar which would vibrate vigorously with the alternating microwave field. In the case of microwave irradiation at 50 W and 200 W, water molecules were partially removed, while the power was not strong enough to remove EG molecules. This facilitated the formation of a new solvation layer containing more EG than water, dispersing the NiCo DHs nuclei and causing the formation of 2D nanosheets after oriented attachment growth. However, generation of NiCo DHs brought an increase in microwave power intensity in the reacting fluid area Thereby, de-EG started to happen leading to the formation of bare

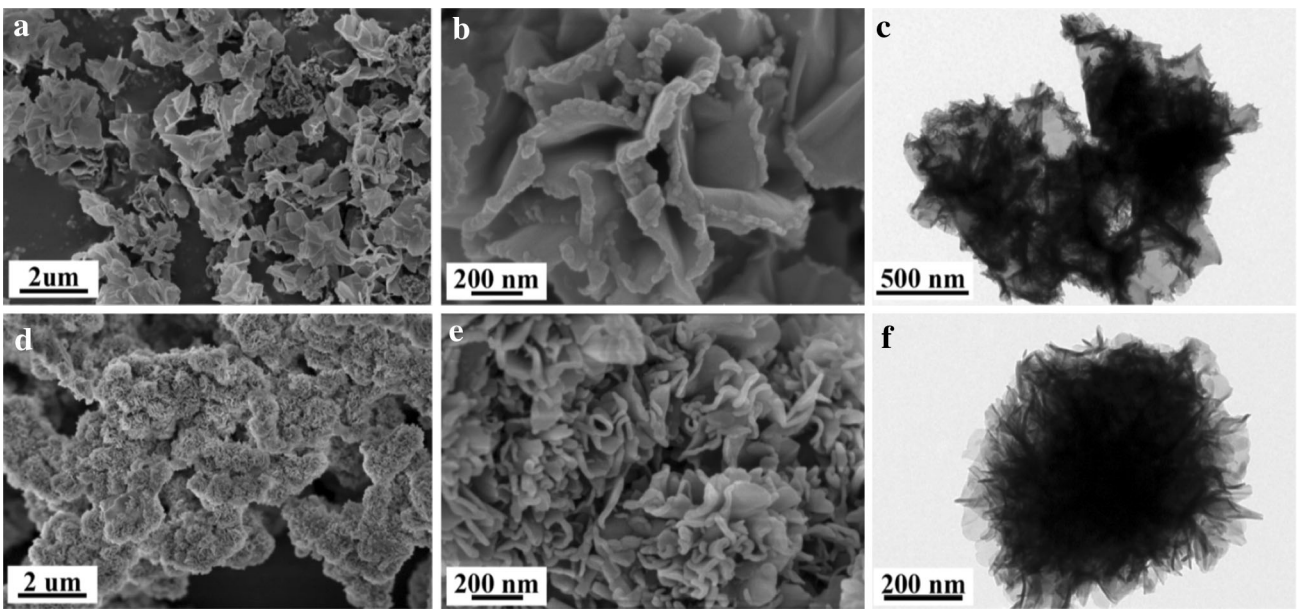

Figure 5 FESEM (**a**, **b**, **d**, **e**) and TEM (**c**, **f**) images of the as-synthesized NiCo DHs harvested from 50 W microwave irradiation (**a**–**c**) and 300 W microwave irradiation (**d**–**f**), respectively.

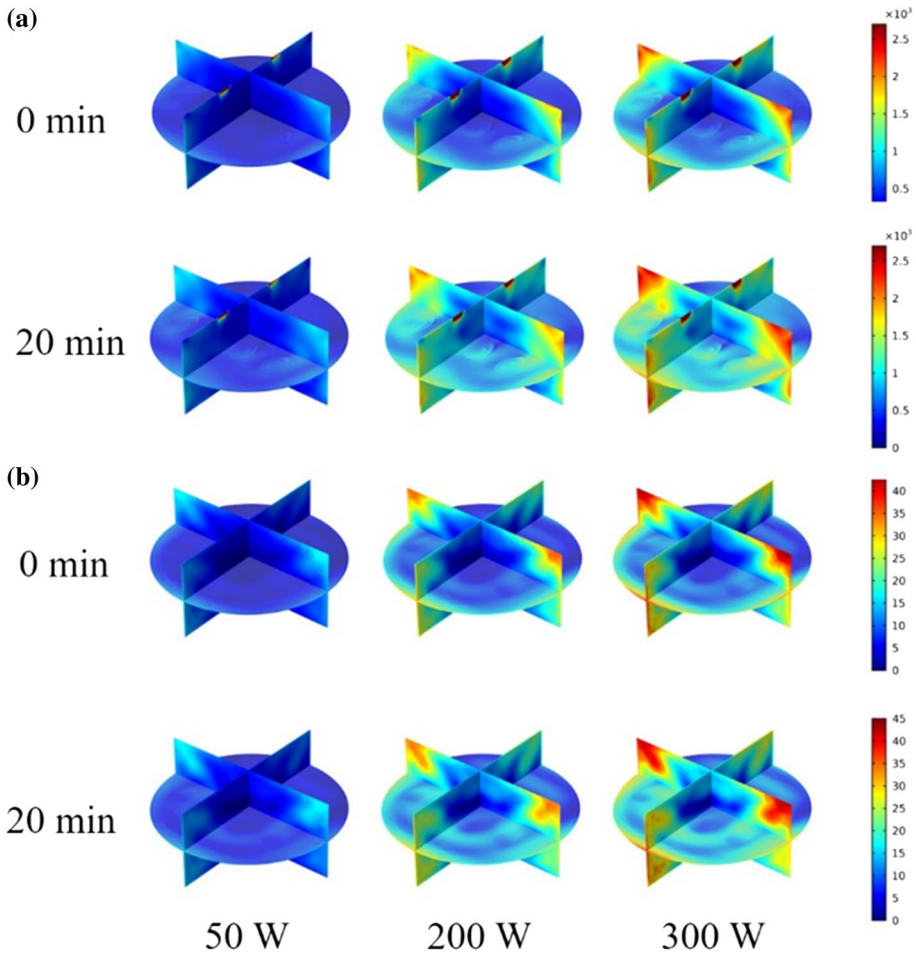

Figure 6 Field strength distribution in the reaction system under different microwave powers and reaction times: **a** electric field; **b** magnetic field.

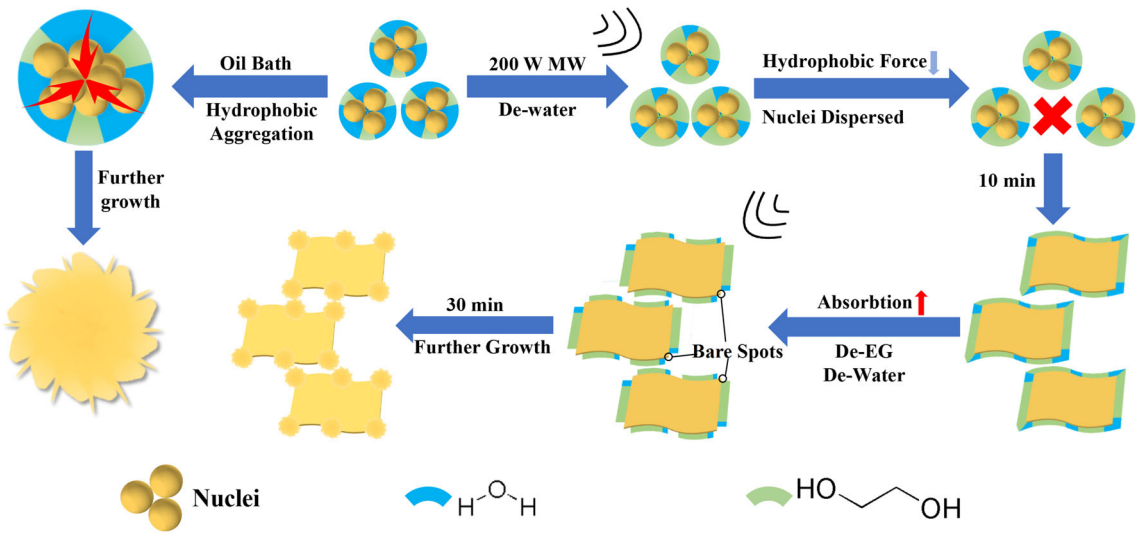

Figure 7 Reaction mechanism of oil bath and microwave assistant.

spots on the NiCo DHs 2D nanosheets, where formation of nanoflower clusters was initiated.

Further, the as-synthesized NiCo DH-OB and NiCo DH-200 MW were applied as electrode materials in supercapacitors as a proof of concept. Figure 8a

shows the Nyquist plots for NiCo DH-200 MW and NiCo DH-OB. As can be seen, slope for NiCo DH-200 MW presented no significant difference with that for NiCo DH-OB, indicating similar ion diffusion speeds which were probably due to similar pore size distribution. Inset of Fig. 8a shows that the diameter of the semicircle for NiCo DH-200 MW was slightly smaller than that of NiCo DH-OB, suggesting smaller charge transfer resistance of NiCo DH-200 MW. Also, the intersection of the Nyquist plot with horizontal axis was smaller for NiCo DH-200 MW than NiCo DH-OB, implying the smaller solution resistance and equivalent series resistance [40]. Figure 8b shows the specific capacity values of both samples at different current densities. As can be seen, NiCo DH-200 MW exhibited higher specific capacity at all current densities. At a current density of 10 A g^{-1}, NiCo DH-200 MW showed a value of 1067 F g^{-1}, which is about 10% higher than 989 F g^{-1} for NiCo DH-OB. As the current density increased to 50 A g^{-1}, the specific capacity value of NiCo DH-OB decreased significantly to 400 F g^{-1}, while the value of NiCo DH-200 MW was 50% higher (615 F g^{-1}), indicating that the microwave-enabled synthesis of flower-on-sheet nanostructure was extremely favorable for energy storage at high current density. The capacitance values of the product are inferior to those of some reported NiCo DHs, which could probably be attributed to the lower Ni/Co ratio and the higher loading of active material (3.8 mg cm^{-2} compared to ~ 2.0 mg cm^{-2} usually loaded by others) [41, 42]. However, it still shows comparable or even slightly higher storage capacitance than many reported Ni_1Co_1 DH and Ni_1Co_2 DH, even though the loading of Ni_1Co_2 DH in this work is relatively high, indicating the superiority of the unique flower-on-sheet nanostructure [12, 37, 41]. It is likely that the 2D substrate ensured a more directed electron transport, while the 3D nanoflower clusters prevented the aggregation of the nanosheets facilitating sufficient interfacial contact between the electrode materials and the electrolyte ions as indicated by the BET results and the Nyquist plot; both factors led to enhanced rate capability. Afterward, the cycling stability of the two samples was examined as shown in Fig. 8c. After 1000 cycles, a capacity retention of 101% and 104% was achieved for NiCo DH-200 MW and NiCo DH-OB, respectively, demonstrating superior stability of both architectures. Based on the above, it can be concluded that microwave field was successfully applied to tune the morphology of NiCo DHs nanostructure to get enhanced energy storage performance.

Conclusion

In this work, we showed a microwave-enabled tuning of NiCo DH morphologies. Unique flower-on-sheet nanostructure of NiCo DH was obtained under certain power of microwave irradiation, while the oil-bath method gave yield to microspheres under the same temperature program. Microwave field intensity and its variation as reaction carried on are key factors in facilitating the formation of the unique nanostructure. When tested as electrode materials in supercapacitor, the NiCo DH flower-on-sheet nanostructure exhibited enhanced specific capacities, especially at high current density.

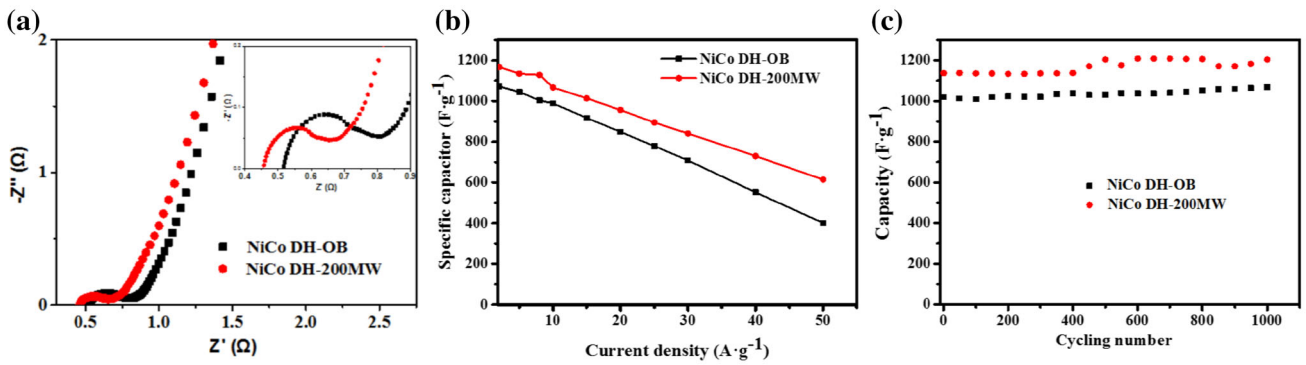

Figure 8 Electrochemical performance of as-synthesized NiCo DH-OB and NiCo DH-200 MW as electrode materials in supercapacitor: **a** the Nyquist plot; **b** the rate capability from 1 to 50 A g^{-1}; **c** stability test at 10 A g^{-1}.

Acknowledgements

This work was supported by the National Natural Science Foundation of China (Grant No. 61731013), State Key Laboratory of Environmental Chemistry and Ecotoxicology, Research Center for Eco-Environmental Sciences, Chinese Academy of Sciences (Grant No. KF2016-26), State Key Laboratory of Efficient Utilization for Low Grade Phosphate Rock and Its Associated Resources (Grant No. WFKF2017-05). The authors also appreciate the technical support for Materials Characterization from The Analytical & Testing Center of Sichuan University.

Compliance with ethical standards

Conflict of interest The authors declare that they have no conflict of interest.

Electronic supplementary material: The online version of this article (https://doi.org/10.1007/s10853-019-03324-y) contains supplementary material, which is available to authorized users.

References

[1] Zhang QF, Uchaker E, Candelaria SL, Cao GZ (2013) Nanomaterials for energy conversion and storage. Chem Soc Rev 42:3127–3171

[2] Liu CJ, Burghaus U, Besenbacher F, Wang ZL (2010) Preparation and characterization of nanomaterials for sustainable energy production. ACS Nano 4:5517–5526

[3] Rossi LM, Costa NJS, Silva FP, Wojcieszak R (2014) Magnetic nanomaterials in catalysis: advanced catalysts for magnetic separation and beyond. Green Chem 16:2906–2933

[4] Zhou ZY, Tian N, Li JT, Broadwell I, Sun SG (2011) Nanomaterials of high surface energy with exceptional properties in catalysis and energy storage. Chem Soc Rev 40:4167–4185

[5] Guo SJ, Wang E (2011) Noble metal nanomaterials: controllable synthesis and application in fuel cells and analytical sensors. Nano Today 6:240–264

[6] Yoon H, Jang J (2009) Conducting-polymer nanomaterials for high-performance sensor applications: issues and challenges. Adv Funct Mater 19:1567–1576

[7] Kannan AM, Munukutla L (2007) Carbon nano-chain and carbon nano-fibers based gas diffusion layers for proton exchange membrane fuel cells. J Power Sources 167:330–335

[8] Yang D, Zhou YP, Rui XH, Zhu JX, Lu ZY, Fong E, Yan QY (2013) Fe_3O_4 nanoparticle chains with N-doped carbon coating: magnetotactic bacteria assisted synthesis and high-rate lithium storage. RSC Adv 3:14960–14962

[9] Morin JF (2014) Carbon nanomaterials from rods to sheets in a flash. Nat Chem 6:463–464

[10] Kim S, Kim JH, Lee JS, Park CB (2015) Beta-sheet-forming, self-assembled peptide nanomaterials towards optical, energy, and healthcare applications. Small 11:3623–3640

[11] Zhang X, Zhou YP, Luo B, Zhu HC, Chu W, Huang KM (2018) Microwave-assisted synthesis of $NiCo_2O_4$ double-shelled hollow spheres for high-performance sodium ion batteries. Nano-Micro Lett 10:1–7

[12] Li J, Wei M, Chu W, Wang N (2017) High-stable alpha-phase NiCo double hydroxide microspheres via microwave synthesis for supercapacitor electrode materials. Chem Eng J 316:277–287

[13] Zhou YP, Rui XH, Sun WP, Xu ZC, Zhou Y, Ng WJ, Yan QY, Fong E (2015) Biochemistry-enabled 3D foams for ultrafast battery cathodes. ACS Nano 9:4628–4635

[14] Zhou YP, Sun WP, Rui XH, Zhou Y, Ng WJ, Yan QY, Fong E (2016) Biochemistry-derived porous carbon-encapsulated metal oxide nanocrystals for enhanced sodium storage. Nano Energy 21:71–79

[15] Lou XW, Archer LA, Yang ZC (2008) Hollow micro-/nanostructures: synthesis and applications. Adv Mater 20:3987–4019

[16] Wang YH, Maspoch D, Zou SL, Schatz GC, Smalley RE, Mirkin CA (2006) Controlling the shape, orientation, and linkage of carbon nanotube features with nano affinity templates. P Natl Acad Sci USA 103:2026–2031

[17] Zhang SL, Yao F, Yang L, Zhang FZ, Xu SL (2015) Sulfur-doped mesoporous carbon from surfactant-intercalated layered double hydroxide precursor as high-performance anode nanomaterials for both Li-ion and Na-ion batteries. Carbon 93:143–150

[18] Naushad M (2014) Surfactant assisted nano-composite cation exchanger: development, characterization and applications for the removal of toxic Pb^{2+} from aqueous medium. Chem Eng J 235:100–108

[19] Meher SK, Rao GR (2011) Ultralayered Co_3O_4 for high-performance supercapacitor applications. J Phys Chem C 115:15646–15654

[20] Horikoshi S, Abe H, Torigoe K, Abe M, Serpone N (2010) Access to small size distributions of nanoparticles by microwave-assisted synthesis. Formation of Ag nanoparticles in aqueous carboxymethylcellulose solutions in batch and continuous-flow reactors. Nanoscale 2:1441–1447

[21] Bilecka I, Niederberger M (2010) Microwave chemistry for inorganic nanomaterials synthesis. Nanoscale 2:1358–1374

[22] Polshettiwar V, Varma RS (2010) Green chemistry by nano-catalysis. Green Chem 12:743–754

[23] Baghbanzadeh M, Carbone L, Cozzoli PD, Kappe CO (2011) Microwave assisted synthesis of colloidal Inorganic nanocrystals. Angew Chem Int Ed 50:11312–11359

[24] Patzke GR, Zhou Y, Kontic R, Conrad F (2011) Oxide nanomaterials: synthetic developments, mechanistic studies, and technological innovations. Angew Chem Int Ed 50:826–859

[25] Zhu YJ, Chen F (2014) Microwave-assisted preparation of inorganic nanostructures in liquid phase. Chem Rev 114:6462–6555

[26] Yang XQ, Wu J, Mao XW, Jamison TF, Hatton TA (2014) Microwave assisted synthesis of cyclic carbonates from olefins with sodium bicarbonates as the C_1 source. Chem Commun 50:3245–3248

[27] Faraji S, Ani FN (2014) Microwave-assisted synthesis of metal oxide/hydroxide composite electrodes for high power supercapacitors—a review. J Power Sources 263:338–360

[28] Gong ZL, Yang Y (2011) Recent advances in the research of polyanion-type cathode materials for Li-ion batteries. Energy Environ Sci 4:3223–3242

[29] Xu X, Liu W, Kim Y, Cho J (2014) Nanostructured transition metal sulfides for lithium ion batteries: progress and challenges. Nano Today 9:604–630

[30] Zhang YF, Li LQ, Su HQ, Huang W, Dong XC (2015) Binary metal oxide: advanced energy storage materials in supercapacitors. J Mater Chem A 3:43–59

[31] Yan HW, Huang XJ, Lu ZH, Huang H, Xue RJ, Chen LQ (1997) Microwave synthesis of $LiCoO_2$ cathode materials. J Power Sources 68:530–532

[32] Liu HX, Hu C, Zhu XJ, Hao H, Luo JR, Zhou J, Ouyang SX (2004) Solid chemical reaction in microwave and millimeter-wave fields for the syntheses of $LiMn_2O_4$ compound. Mater Chem Phys 88:290–294

[33] Gao LB, Surjadi JU, Cao K, Zhang HT, Li PF, Xu S, Jiang CC, Song J, Sun D, Lu Y (2017) Flexible fiber-shaped supercapacitor based on nickel–cobalt double hydroxide and pen ink electrodes on metallized carbon fiber. ACS Appl Mater Interfaces 9:5409–5418

[34] Li XC, Shen JJ, Sun W, Hong XD, Wang RT, Zhao XH, Yan XB (2015) A super-high energy density asymmetric supercapacitor based on 3D core-shell structured NiCo-layered double hydroxide@carbon nanotube and activated polyaniline-derived carbon electrodes with commercial level mass loading. J Mater Chem A 3:13244–13253

[35] Li M, Ma KY, Cheng JP, Lv DH, Zhang XB (2015) Nickel–cobalt hydroxide nanoflakes conformal coating on carbon nanotubes as a supercapacitive material with high-rate capability. J Power Sources 286:438–444

[36] Kappe CO (2008) Microwave dielectric heating in synthetic organic chemistry. Chem Soc Rev 37:1127–1139

[37] Zhang J, Cheng JP, Li M, Liu L, Liu F, Zhang XB (2015) Flower-like nickel–cobalt binary hydroxides with high specific capacitance: tuning the composition and asymmetric capacitor application. J Electroanal Chem 743:38–45

[38] Xu J, Dong YZ, Cao JY, Guo B, Wang WC, Chen ZD (2013) Microwave-incorporated hydrothermal synthesis of urchin-like $Ni(OH)_2$–$Co(OH)_2$ hollow microspheres and their supercapacitor applications. Electrochim Acta 114:76–82

[39] Yan T, Li ZJ, Li RY, Ning Q, Kong H, Niu YL, Liu J (2012) Nickel–cobalt double hydroxides microspheres with hollow interior and hedgehog-like exterior structures for supercapacitors. J Mater Chem 22:23587–23592

[40] Sun HT, Mei L, Liang JF et al (2017) Three-dimensional holey-graphene/niobia composite architectures for ultrahigh-rate energy storage. Science 356:599–604

[41] Chen H, Hu LF, Chen M, Yan Y, Wu LM (2014) Nickel–cobalt layered double hydroxide nanosheets for high-performance supercapacitor electrode materials. Adv Funct Mater 24:934–942

[42] Xia DD, Chen HC, Jiang JJ, Zhang L, Zhao YD, Guo DP, Yu WJ (2015) Facilely synthesized a phase nickel–cobalt bimetallic hydroxides: tuning the composition for high pseudocapacitance. Electrochim Acta 156:108–114